DOI 10.1007/s11182-019-01864-z

Russian Physics Journal, Vol. 62, No. 8, December, 2019 (Russian Original No. 8, August, 2019)

STRUCTURE AND PHASE COMPOSITION OF Ti–6Al–4V ALLOY OBTAINED BY ELECTRON-BEAM ADDITIVE MANUFACTURING

V. R. Utyaganova, A. V. Vorontsov, A. A. Eliseev, K. S. Osipovich, K. N. Kalashnikov, N. L. Savchenko, V. E. Rubtsov, and E. A. Kolubaev

UDC 621.9.048.7 + 539.512

The paper presents the fabrication of Ti–6Al–4V *alloy specimens using two operating modes of the electron beam additive manufacturing (EBAM). The structure, phase composition and microhardness of the obtained alloy specimens are investigated. The EBAM process includes a deposition of* Ti–6Al–4V *wire onto a substrate comprising of VT1-0 (grade 2) titanium alloy and 12Kh18N10 (AISI 321) stainless steel. It is shown that at a high electron beam current, the height and width of the β-phase columnar grains are lower than at a low electron beam current. This phenomenon is discussed in terms of stabilization of the temperature gradient and the increased cooling rate during the building process. This phenomenon is caused by the formation of* Fe_2Ti*,* FeTi *and* Cr_2Ti *intermetallic phases in the diffusion bonding appeared between the titanium and stainless steel plates.*

Keywords: additive manufacturing, titanium alloy, microstructure, microhardness.

INTRODUCTION

Owing to its high strength and corrosion-resistance properties, Ti–6Al–4V alloy is widely used in aerospace, automobile, biomedical and chemical industries [1, 2]. The high cost of titanium components is determined by the high material consumption when machining. Additive manufacturing assists in the cost reduction of titanium alloy products [3] due to manufacturing precision workpieces which require minimum machining. The main requirement for manufacturing precision workpieces is preservation of high properties of the materials obtained.

In additive manufacturing which is highly efficient, the metallic feedstock is typically wire [3]. There are however, difficulties which restrict its wide applications for titanium alloys. High heat intake and high temperature gradient in depositing Ti–6Al–4V wire lead to the formation of columnar grains in β-phase, which are oriented along the deposition direction, normal to the substrate. The formation of β-phase columnar grains is a key factor which determines anisotropy of mechanical properties of titanium products. Under vertical tension (in the deposition direction), the material tends to be more plastic, but displays lower yield stress and ultimate strength, than under horizontal tension, parallel to the substrate [4]. Such a material structure is inadmissible for products which require isotropic mechanical properties. Nevertheless, the structure with coarse columnar grains in β-phase can be used in fabricating products requiring highly anisotropic mechanical properties.

As of now, several investigations have been conducted, which attempted to reduce the size of columnar grains in titanium alloy fabricated by the additive manufacturing. Colegrove, *et al*. [5] built Ti–6Al–4V structure with small β-phase grains by using high roll pressure for each as-deposited layer. Wu, *et al*. [6] used the increased cooling rate to reduce the grain size in β-phase. In [7], Bermingham, *et al*. managed to generate narrow columnar grains of β-phase

Institute of Strength Physics and Materials Science of the Siberian Branch of the Russian Academy of Sciences, Tomsk, Russia, e-mail: veronika_ru@ispms.tsc.ru; vav@ispms.ru; alan@ispms.tsc.ru; osipovich_k@ispms.tsc.ru; sso.spektr.asu@gmail.com; savnick@ispms.tsc.ru; rvy@ispms.tsc.ru; eak@ispms.tsc.ru. Translated from Izvestiya Vysshikh Uchebnykh Zavedenii, Fizika, No. 8, pp. 143–150, August, 2019. Original article submitted June 25, 2019.

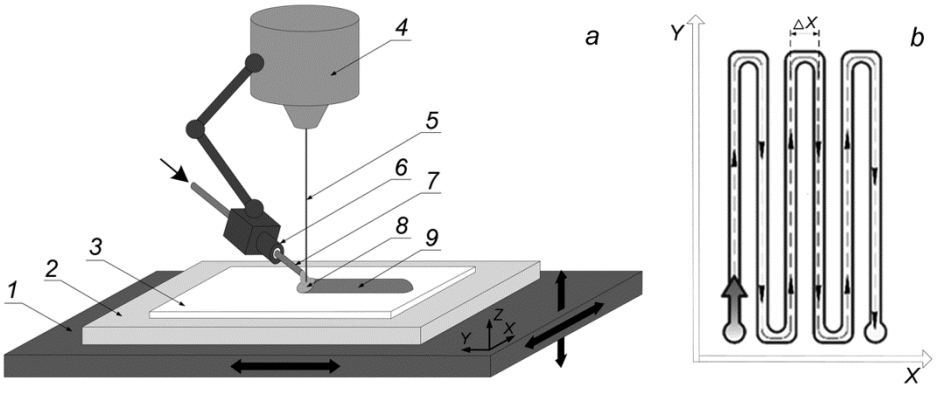

Fig. 1. Schematic of EBAM process (*a*) and build direction (*b*): *1* – build platform, *2* – AISI 321 steel substrate, *3* – grade 2 titanium prior deposit (substrate), *4* – electron beam gun, *5* – electron beam, *6* – wire feeder, *7* – wire, *8* – molten alloy puddle, *9* – re-solidified alloy.

through the addition of boron particles to the molten alloy puddle. Not all of these grain-reduction methods apply to the wire-fed electron beam additive manufacturing (EBAM) technology because the process of making products occurs in a vacuum chamber. Nevertheless, the EBAM technology has great potential for the production of materials with a unique structure and high mechanical properties [8].

This work focuses on the investigation of the structure and phase composition of Ti–6Al–4V alloy produced by the wire-fed electron beam manufacture process and built on a substrate comprising of VT1-0 (grade 2) titanium alloy and 12Kh18N10 (AISI 321) stainless steel. The aim of this work is to determine the process parameters which provide the formation of the diffusion bonding between the titanium and stainless steel plates, which, in turn, changes the cooling conditions of Ti–6Al–4V alloy deposition and modifies the columnar structure of β-phase grains.

MATERIALS AND METHODS

The alloy specimens were produced on the experimental setup intended for building products using the wire-fed EBAM process in a vacuum environment. The electron beam was used to provide the molten alloy puddle and wire melting. The general arrangement drawing for the manufacturing process is given in Fig. 1*a*. Ti–6Al–4V wire with a diameter of 0.8 mm was used as a feedstock. The alloy specimens were built on a substrate comprising a 75 × 75 × 2.5 mm grade 2 titanium plate and a 110 × 110 × 7.8 mm AISI 321 steel plate. During the deposition process, the molten alloy puddle was formed by the surface scanning with a circular electron beam 5 mm in diameter. The scanning frequency was 1 kHz. The wire feedstock was conveyed from the wire-feed system, which was fixed relatively the electron beam gun as shown in Fig. 1*a*. The electron beam parameters, the wire feeding speed and the travel speed (the ratio between the build platform motion and the beam direction) were combined so that to ensure the stability of the wire melting process and a continuous flow of the molten alloy into the molten puddle.

The EBAM parameters are gathered in Table 1. The two EBAM modes differ from each other by a twofold increase in the beam current. According to the scanning procedure illustrated in Fig. 1*b*, three substrates are deposited onto the build platform.

The specimens were prepared for metallographic examination using the automated grinding and polishing techniques. At first, the specimens were ground with abrasive papers and then polished with diamond paste. The final chemical polishing was carried out using a 2 wt.% HF–2 wt.% HNO_3–96 wt.% H_2O etchant in order to obtain a desired surface.

TABLE 1. EBAM Parameters

Beam accelerating voltage	Mode 1	Mode 2
	40 kV	
Beam current: – first layer – successive layers	 16 mA 14 mA	 30 mA 28 mA
Beam diameter	0.15–0.18 mm	
Focal length	220 mm	
Beam scanning	5 mm diameter	
Scanning frequency	1 kHz	
Scan step ΔX	5 mm	
Layer height	0.8 mm	
Number of layers	3	
Feeding rate	880 mm /min	
Guidewire angle of inclination relative to substrate	25 degrees	
Guidewire angle of inclination relative to *X*-axis	45 degrees	
Travel speed	220 mm /min	

The microstructure analysis was undertaken on the polished samples with an optical microscope and a scanning electron microscope equipped with an electron probe microanalyzer (EPMA). Phase identification was performed through the X-ray diffraction (XRD) analysis using Co-K_α radiation.

RESULTS AND DISCUSSION

In Fig. 2 metallography images are obtained in *Z*–*Y* plane. The structure of Ti–6Al–4V specimen manufactured in mode 1 consists of epitaxial columnar grains which grow through the deposited layers. The grains are inclined relative to the deposition direction (*Z*-axis). The structure of Ti–6Al–4V specimen manufactured in mode 2 also consists of columnar grains, but more ground as compared to mode 1. The quantitative metallography data on the columnar grain size are summarized in Table 2.

The XRD patterns presented in Fig. 3 are obtained for Ti–6Al–4V specimens built in two EBAM modes. The diffraction peaks of both modes match α-phase. The ratio *c*/*a* of the lattice parameters is usually used to detect the potential presence of both α- and α′-phases in titanium specimens [9]. When the lattice parameters are changed such that $a = 2.93$ Å, $c = 4.57$ Å and $c/a = 1.595$ for mode 1 and $a = 2.94$ Å, $c = 4.67$ Å and $c/a = 1.590$ for mode 2, α-phase can be identified as martensite α′-phase, which forms inside the primary columnar grains of β-phase. At room temperature, this β-phase does not leave even a weak (110) reflection as shown in Fig. 3*b*. Therefore, the volume fraction of the β-phase residue is less than 5% for all the Ti–6Al–4V specimens produced.

As reported in [9], α-phase is present when $c/a = 1.5964$. Hence, in addition to martensite α′-phase, the higher *c*/*a* ratio in Ti–6Al–4V specimens generated by mode 1 indicates to the α-phase formation from β-phase by the diffusion mechanism. This is due to the temperature-driven cooling rate of β-to-α phase transition, which is lower as compared to mode 2.

The microstructure shown in Fig. 4 consists of martensite α′-phase with orthogonal, elongated lamellas. Such a structure is characteristic to specimens built under both modes and it forms inside the preceding β-phase columnar grains. The quantitative metallography analysis shows that in each wire deposit, the thickness of α′-phase lamellas in Ti–6Al–4V specimens built in mode 2 is lower than in specimens built in mode 1. For comparison the reader is referred to Table 3. Al-Bermani, *et al*. [10] demonstrate that if in producing Ti–6Al–4V-like alloys the temperature is below the β-to-α phase transition (995°C), β-phase transforms to α-phase. If the cooling rate exceeds the critical value of 410 K/s, β-phase transforms to martensite α′-phase. Owing to high cooling rates specific to additive manufacturing (10^2–10^5 K/s

TABLE 2. Average Size of Columnar Grains in Ti–6Al–4V Specimens

Planes	Grain size, mm			
	Mode 1		Mode 2	
	Height	Width	Height	Width
Z–X	1.58 ± 0.75	0.64 ± 0.25	0.72 ± 0.49	0.59 ± 0.38
Z–Y	1.35 ± 0.63	0.68 ± 0.43	0.5 ± 0.38	0.46 ± 0.31

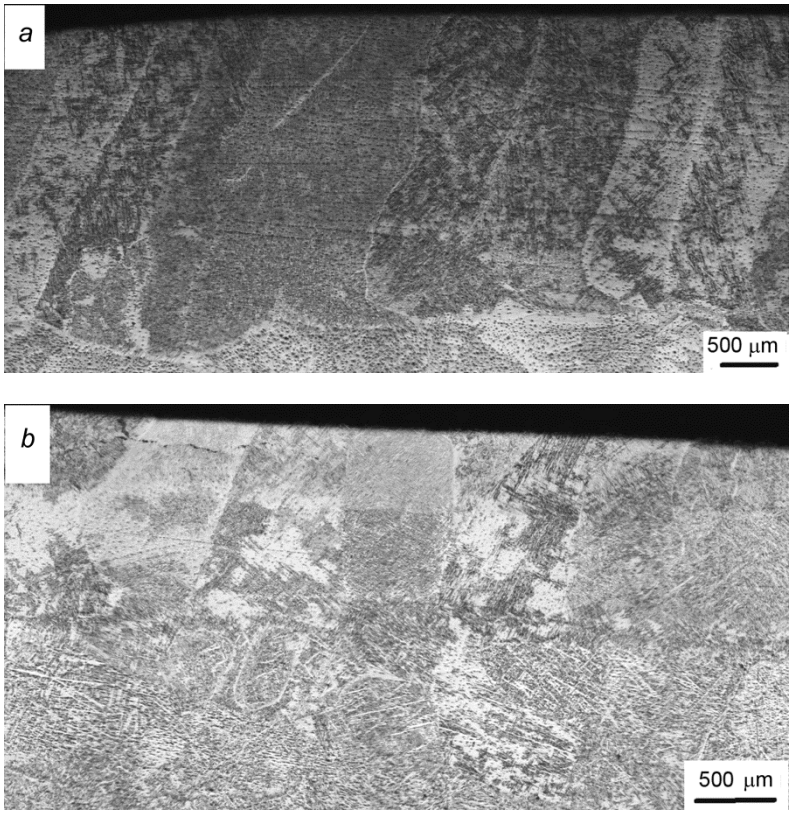

Fig. 2. Metallography images of the microstructure of Ti–6Al–4V specimen built perpendicular to the deposition direction (*Z–Y* plane): *a* – mode 1, *b* – mode 2.

[3]), martensite α′-phase often occurs inside β-phase grains. In the case of high cooling rate, the α′-phase nucleation occurs in several places at a time. They merge and generate a completed network of thin martensite layers [10]. The thickness of these layers depends on the cooling rate and the β-to-α phase transition temperature. A high cooling rate results in the formation of thinner α′-phase lamellas, and *vice versa* [10].

The absence of β-phase in the XRD patterns and the observed structure of α-phase orthogonal lamellas indicate that both modes of the wire deposition are characterized by rather a high cooling rate in the temperature range below the β-to-α phase transition temperature. At the same time, in mode 2 the cooling rate in this temperature range is higher than in mode 1, that is proved by the lower degree of α-phase tetragonality and the lower thickness of martensite lamellas in the produced Ti–6Al–4V specimens.

Ti–6Al–4V specimens built in mode 2 show the formation of the diffusion bonding between the titanium and steel plates. In turn, Ti–6Al–4V specimens built in mode 1 have no such a bonding, and lamellas separate from each other after the electrical discharge machining of the specimens.

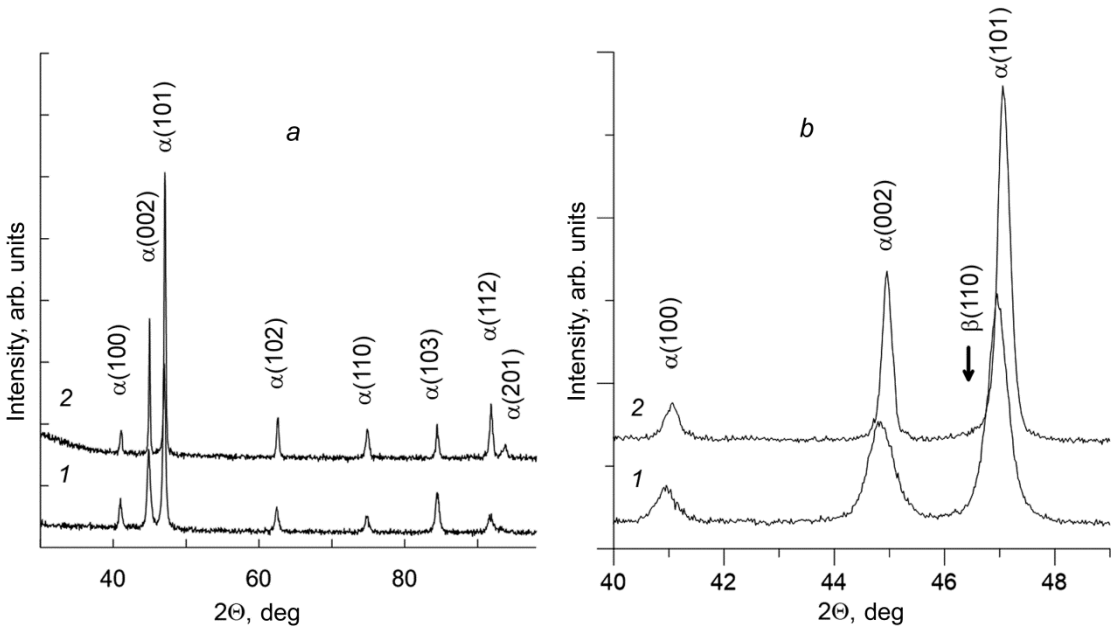

Fig. 3. XRD patterns of Ti–6Al–4V specimens produced in mode 1 (curve *1*) and mode 2 (curve *2*).

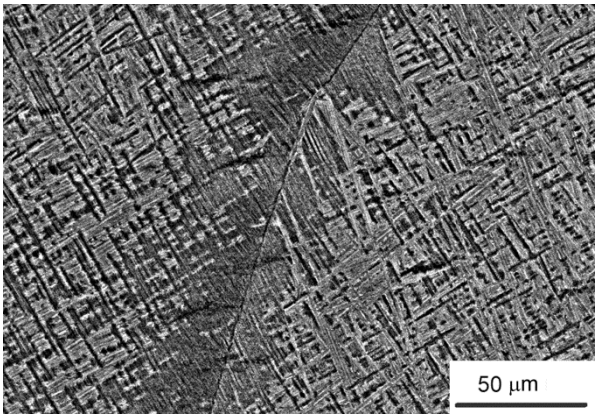

Fig. 4. Metallography image of Ti–6Al–4V specimen microstructure consisting of martensite α′-phase with orthogonal, elongated lamellas inside the preceding β-phase columnar grains.

The electron backscatter diffraction technique used for scanning electron microscopy (SEM) observations helps to study the crystal structure of specimens in the diffusion bonding between the titanium and steel plates. According to the SEM image of the diffusion bonding shown in Fig. 5, there are two interlayers between the titanium plate (zone 1) and the steel plate (zone 4). Interlayer 2 adjacent to the titanium plate is brighter, 10 μm thick. Interlayer 3 is 70 μm thick and joins the steel plate. This interlayer has a complex structure consisting of bright inclusions of phases.

As is known, when titanium and titanium alloy steel are heated in vacuum, intermetallic phases form between such elements as Fe, Ti and Cr. The effect from Ni, Al, Cu and Mn elements is ignored due to their very low concentration [11]. The electron probe microanalysis of all the four zones shown in Fig. 5 is carried out to identify the phase composition of the interlayers. The EPMA results are given in Table 4. Zones 1 and 2 are enriched with titanium, the latter having the increased content of Cr and Fe. According to [11], Fe, Ni, Cr and Cu elements stabilize β-phase in

TABLE 3. Thickness of α′-Phase Lamellas in Ti–6Al–4V Specimens

Martensite lamellas	Lamella thickness, μm	
	Mode 1	Mode 2
3	1.37 ± 0.43	1.13 ± 0.42
2	1.84 ± 0.55	1.35 ± 0.36
1	2.7 ± 0.83	1.6 ± 0.38

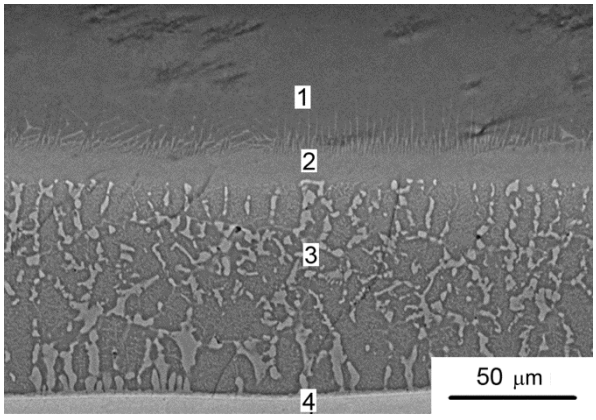

Fig. 5. SEM image of the diffusion bonding between the titanium and steel plates formed in operating mode.

titanium. During the formation of the diffusion bonding between the titanium alloy and stainless steel these elements migrate from the latter to the former, the high-temperature β-phase being preserved in titanium even at room temperature [11]. In our case, interlayer 2 probably consists of β-phase stabilized by Fe, Ni, Cr elements. At the same time, at the interface between 1 and 2 zones the bright lamellas of titanium β-phase appear in the darker matrix of titanium α-phase, which correspond to the (α+β) phase structure formed due to the insufficient amount of stabilizing elements (Fe, Ni, Cr). This is in agreement with observations made in [11]. Based on the proportion of the chemical elements gathered in Table 4, interlayer 3 consists of intermetallic phases formed during heating and deposition of Ti–6Al–4V specimen. The EPMA results of the bright and dark phase inclusions show the proportion of the chemical elements specific to Fe_2Ti, Cr_2Ti and FeTi phases, respectively.

To provide more reliable identification of phases formed in the diffusion bonding between the titanium and steel plates, this bonding was destructed to conduct the XRD analysis. This analysis showed that along with phases presenting the initial titanium alloy and stainless steel, there were such reaction products as FeTi, Fe_2Ti and Cr_2Ti intermetallic phases and also Ti β-phase.

As is known, the increase in the bonding temperature and the period of its existence lead to the atom migration through the interface, which affects the thickness of the reaction layers [11]. We do not measure the deposition temperature of Ti–6Al–4V specimens in this work. It can, however, be estimated by the comparison of the thickness of the formed reaction layers and the similar layers obtained in [10]. Such structures usually occur after 850–900°C diffusion bonding of titanium alloy and stainless steel plates lasting for one hour [11].

In Fig. 6 one can see the dependence between the Vickers microhardness and the distance to the specimen apex, which is considered as a zero point. The highest hardness of the specimen built in mode 1 is observed near its apex, which then decreases with increasing distance from the apex and lowers to the hardness value of the titanium substrate. The hardness of the specimen built in mode 2 is almost unchanged throughout the distance from its apex to the titanium substrate. But owing to solid and fragile intermetallic phases nearby the steel-alloy interface its hardness dramatically grows up to 12 GPa [11].

TABLE 4. EPMA-Based Chemical Composition

Zones	Chemical composition, at.%					
	Al	Ti	V	Cr	Fe	Ni
1	2.3	95.7	–	0.6	0.7	Balance
2	–	93.5	–	3.0	3.5	Balance
3	6.8	54.6	–	11.9	24.2	Balance
4	3.4	7.8	0.8	28.7	59.4	Balance

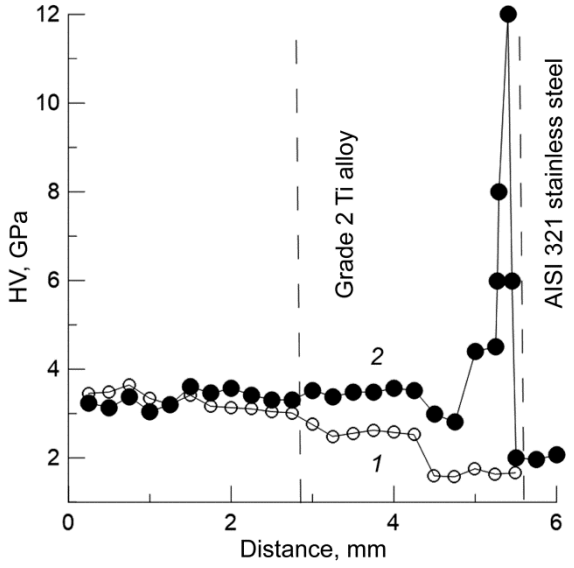

Fig. 6. Dependences between the Vickers microhardness and the height of Ti–6Al–4V specimens: *1* – mode 1, *2* – mode 2.

Two factors that affect the grain growth during the EBAM process are commonly known as the temperature gradient and cooling rate. The high temperature gradient and the low cooling rate are likely to assist in the formation of columnar grains, whereas the low temperature gradient and the high cooling rate lead to the formation of equiaxed grain structure [12, 13]. Moreover, in titanium alloys the size of preceding β-phase columnar grains is determined mostly by the time of their existence in between the liquidus and the β-to-α phase transition temperature (995°C for Ti–6Al–4V alloy) [14].

The formation of the large columnar structure during mode 1 is predictable, because in Ti–6Al–4V specimen built by using both laser and electron beam sources, the similar structures have been also formed due to the high temperature gradients [10]. And the results of structural investigations of Ti–6Al–4V specimen built in mode 2 turn to be unexpected because despite the increased input energy, the columnar structure is crushed.

Titanium and stainless steel have the low thermal conductivity of about 16 W/(m·K) at room temperature. At the same time, the thermal conductivity of the obtained intermetallics is much higher. In particular, for FeTi intermetallic compound it is ~73 W/(m·K) [15]. Consequently, when the deposition process occurs in mode 1, the observed high temperature gradient is conditioned by the heat accumulation in the lower wire deposits due to the low thermal conductivity of the titanium substrate. The material is exposed to heat in the same way as to isothermal annealing at about 850–900°C, which contributes to the growth in the lamella thickness of α′-phase (see Table 3) and the formation of α-phase *via* the diffusion mechanism. The upper wire deposits are cooled relatively fast, thereby creating conditions for the formation of coarse and elongated β-phase columnar grains (see Fig. 2*a*). When the deposition process occurs in mode 2, the increase beam current promotes a rapid formation of the diffusion bonding

between titanium and stainless steel. Owing to high conductivity, the built intermetallic deposits effectively remove heat from the earlier built deposits, thereby decreasing the temperature gradient and enhancing the cooling rate. Such processes lead to the increase in the number of crystallization centres, and thus both of these factors have positive implications for the formation of equiaxed grain structure of β-phase in Ti–6Al–4V alloy (see Fig. 2*b*). Consequently, the microhardness of Ti–6Al–4V alloy built in mode 2 does not change with the growing height of wire deposits (Fig. 6).

CONCLUSIONS

The structure, phase composition and microhardness were investigated in Ti–6Al–4V alloy specimens produced by the wire-fed EBAM technology using two operating modes with different beam current. The alloy specimens were produced on the substrate comprising of grade 2 titanium and AISI 321 stainless steel plates.

It was shown that in the high-current operating mode, the height and width of the β-phase columnar grains were lower than in the lower-current mode. The thickness of α′-phase lamellas in each wire deposit produced by the high-current mode was less than that in wire deposits produced in the low-current mode.

The observed modification of the columnar structure in Ti–6Al–4V specimens produced by the high-current mode can be explained by stabilization of the temperature gradient and increased cooling rate due to the formation of Fe_2Ti, FeTi and Cr_2Ti intermetallic phases in the diffusion bonding between the titanium and steel plates.

It was found that grinding of β-phase columnar grains was caused by the formation of the diffusion bonding containing intermetallics. This effect can be used to control the structure of metallic products manufactured by the EBAM technology. Based on a variety of intermetallics forming between the plates made of different metal and alloys, the development of the proposed approach will allow to achieve additional interesting results.

This work was performed within the frame of the Fundamental Research Program of the State Academies of Sciences for 2013-2020, research line III.23.

REFERENCES

1. D. Banerjee and J. C. Williams, Acta Mater., **61**, No. 3, 844–879 (2013).
2. A. V. Panin, M. S. Kazachenok, O. B. Perevalova, *et al.,* Phys. Mesomech., **21**, No. 5, 441–451 (2018).
3. S. Singh, S. Ramakrishna, and R. J. Singh, J. Manuf. Process., **25**, 185–200 (2017).
4. Z. Li, C. Liu, T. Xu, *et al.,* Mater. Sci. Eng., **A742**, 1–26 (2018).
5. P. A. Colegrove, H. E. Coules, J. Fairman, *et al.,* J. Mater. Process. Tech., **213**, No. 10, 1782–1791 (2013).
6. Q. Wu, J. Lu, C. Liu, *et al.,* Materials, **10**, No. 7, 1–11 (2017).
7. M. J. Bermingham, D. Kent, H. Zhan, *et al.,* Acta Mater., **91**, 289–303 (2015).
8. J. Fuchs, C. Schneider, and N. Enzinger, Weld. World, **62**, No. 2, 267–275 (2018).
9. F. Lia, J. Z. Park, J. S. Keist, *et al.,* Mater. Sci. Eng., **A717**, 1–10 (2018).
10. S. S. Al-Bermani, M. L. Blackmore, W. Zhang, *et al.,* Metall. Mater. Trans. A, **41**, No. 13, 3422–3434 (2010).
11. S. Kundu, D. Roy, S. Chatterjee, *et al.,* Mater. Design, **37**, 560–568 (2012).
12. H. Z. Fu and L. Liu, Mater. Sci. Forum, **475–479**, 607–612 (2005).
13. Li Z., Liu C., Xu T., *et al.,* Mater. Sci. Eng. A, **742**, 287–294 (2018).
14. N. Stanford and P. S. Bate Acta Mater., **52**, No. 17, 5215–5224 (2004).
15. Y. Terada, K. Ohkubo, K. Nakagawa, *et al.,* Intermetallics, **3**, 341–355 (1995).